Roughness conformity during tungsten film growth: An *in situ* synchrotron x-ray scattering study

Luca Peverini and Eric Ziegler
European Synchrotron Radiation Facility, Boîte Postale 220, 38043 Grenoble Cedex, France

Thierry Bigault
Institut Laue-Langevin, Boîte Postale 156, 38042 Grenoble Cedex, France

Igor Kozhevnikov
Institute of Crystallography, Leninsky Prospect 59, Moscow 119333, Russia
(Received 23 September 2004; revised manuscript received 21 March 2005; published 25 July 2005)

The spatial and temporal evolution of the surface of a tungsten film deposited by magnetron sputtering is investigated *in situ* and in real time by an x-ray scattering technique. The evolution of roughness is described in terms of its power spectral density and derived from scattering measurements performed using synchrotron x-rays at the energy of 17.5 keV. The data are analyzed in the frame of the first-order perturbation theory, which does not require any model of film growth and correlation function. The approach allows extracting quantitatively both the degree of conformity and the evolution of the in-plane characteristic length of the replication as a function of the growing film thickness.

DOI: 10.1103/PhysRevB.72.045445 PACS number(s): 68.35.Ct, 78.70.Ck, 81.15.Cd

I. INTRODUCTION

Artificial thin films and layered systems are widely used in materials science, optics, and microelectronics. To improve their performance it is essential to understand the roughening and smoothing mechanisms that occur during growth,[1,2] which are eventually responsible for their morphology and surface topology. Studies on thin film growth are frequently performed by an interruption of the process and subsequent *ex situ* characterization using, for example, x-ray scattering[3] (XRS) or local probe techniques,[4] such as atomic force microscopy (AFM) or scanning tunneling microscopy (STM). However, with the synchrotron radiation sources presently available, thin film growth can also be studied *in situ* using XRS-based techniques. In the case of *ex situ* characterization, a number of shortcomings inherent either to the experimental procedure or to the data treatment can be found in the present literature. First, the evolution of roughness upon film growth is usually derived from the analysis of *ex situ*, in-air experiments using a set of samples, each having received a particular treatment. As demonstrated by Underwood *et al.*,[5] the oxidation of a sample surface often results in the development of greater roughness as compared to that of the as-deposited state. Moreover, the use of a series of samples may result in additional errors (artifacts). For example, Asadchikov *et al.*[6] have found a substantial distribution in the statistical parameters describing roughness for silica substrates, although polished under identical technological conditions. Over the same range of spatial frequency, the root mean square (rms) roughness varied from 0.16 nm to 0.21 nm and the Hurst exponent[7] (H) from 0.05 to 0.1. Second, local probe techniques do not permit the extraction of direct information about the cross-correlation (conformity) between the roughness of a film and its substrate. Therefore, a model for film growth is necessary. Finally, the analysis of the XRS data is often based on the distorted-wave Born approximation (DWBA) formalism, in which the interrelation between the roughness correlation functions for the various film interfaces and the scattering diagram is contained in an integral equation. Usually the form of the autocorrelation function at each interface as well as the cross-correlation function must then be postulated. Here, also, a growth model must be chosen *a priori* with a great number of unknown parameters to be adjusted through a fitting procedure.[8–10] To circumvent this problem, a formalism called "first-order perturbation theory" (PT) can be used, in which the scattering amplitude is decomposed as a series on the roughness height.[11]

A film deposited onto a substrate has two interfaces, each with a roughness profile described by random functions $z=\zeta_s(\boldsymbol{\rho})$ and $z=h+\zeta_f(\boldsymbol{\rho})$, where h is the average film thickness and $\boldsymbol{\rho}$ the vector lying in the plane of the surface. The optical properties of a thin film are then determined by three correlation functions defined as $C_s(\rho)=\langle\zeta_s(\rho)\zeta_s(0)\rangle$, $C_f(\rho)=\langle\zeta_f(\rho)\zeta_f(0)\rangle$, and $C_{sf}(\rho)=\langle\zeta_s(\rho)\zeta_f(0)\rangle$. The autocorrelation functions $C_s(\rho)$ and $C_f(\rho)$ describe the statistical properties of the substrate and the external surface of the film, whereas the cross-correlation function $C_{sf}(\rho)$ determines the statistical relationship, namely the conformity, between these two interfaces. Roughness can equivalently be described through the power spectral density (PSD) function that is the Fourier transform of the correlation function. This is the quantity that is effectively measured in scattering experiments.[12] One particular advantage of using the PT approach[13] is its ability to describe the overall evolution of the film roughness in terms of its PSD functions, unambiguously, uniquely, and without any model of thin film roughness or film growth.

In this paper we present results on the growth of tungsten films that are free from the shortcomings listed above. The experiments performed required the development of a set up devoted specifically to the real-time XRS *in situ* investigation of film growth.

 ©2005 The American Physical Society

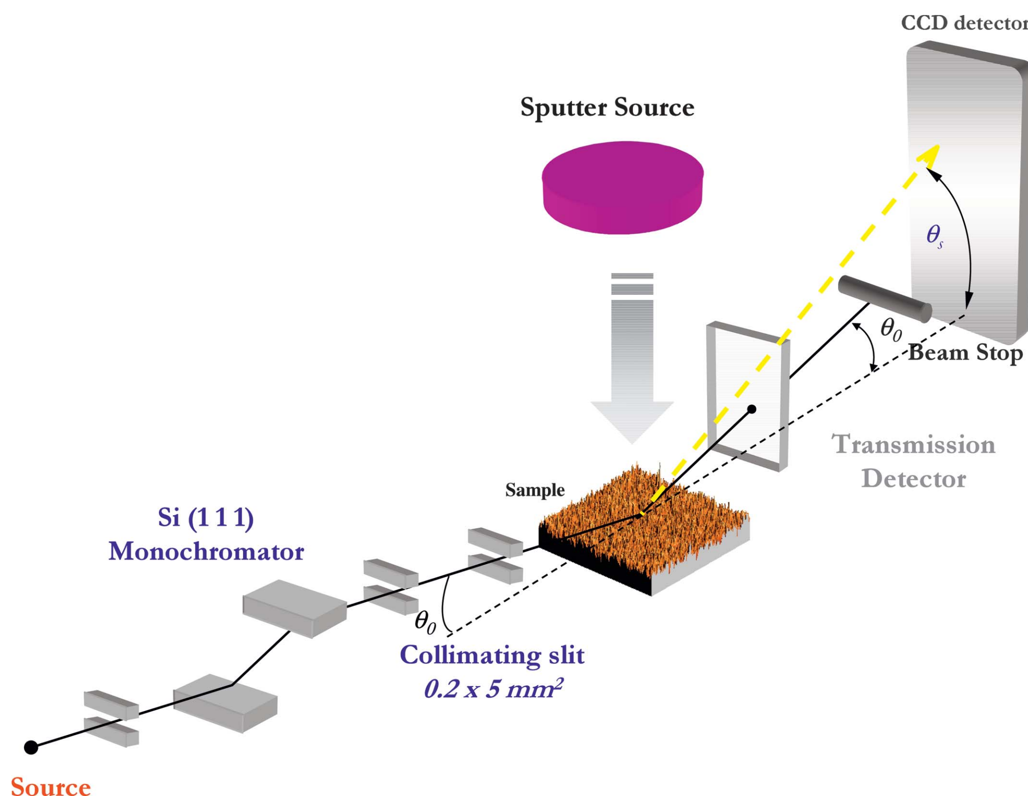

FIG. 1. (Color) Sketch of the experimental set up.

II. REAL-TIME XRS, *in situ* SET UP AND EXPERIMENTAL CONDITIONS

An experimental facility for real-time *in situ* x-ray scattering measurements was developed and installed at the European Synchrotron Radiation Facility (ESRF) bending-magnet beamline BM5. An extended description of this beamline is given elsewhere.[14] A sketch of the experimental set up is shown in Fig. 1. The set up integrates two schemes: sample processing and x-ray detection. A vacuum chamber with a base pressure of 10^{-7} hPa is equipped with a magnetron sputter source for film deposition. Facing the sputter target, the sample is rigidly fixed inside the chamber, so that the degrees of freedom necessary to align the sample surface with respect to the incident x-ray beam (three translations and two tilt angles) are placed on the chamber itself. Then, once the sample is aligned, the chamber remains stationary during film deposition. Two polyamide windows, 150 μm thick, allow the x-ray probe beam to pass through the chamber. Two superpolished silicon substrates were coated with tungsten films by dc magnetron sputtering in a 7×10^{-3} hPa argon pressure using a 30 mA dc current and a 370 V voltage, leading to a typical deposition rate of 7.65 pm/sec. The first detection system, consisting of a silicon *p*-*i*-*n* diode detector, monitors the total intensity of the reflected beam. The second one, composed of a cryogenically cooled charge-coupled device (CCD) camera (1024×256 pixels, pixel size: 19 μm) collects the scattered beam. Here the x-ray photons are converted into visible light by a phosphor screen fiber-coupled optically with the entrance window of a 5:1 reducing-image intensifier. Finally, the intensifier output is imaged onto the CCD detector by a lens system. A beamstop, placed in front of the detector, blocks the intense beam reflected in the specular direction and prevents the detector from saturation. In the experiments described below, the sample-detector distance was set to 1 m. Using a double-crystal monochromator and a set of collimating slits, the probe beam impinging at the sample was set to an energy of 17.5 keV. The divergence in vertical direction was 3×10^{-6} rad and the spectral purity $\Delta E/E$ was of the order of 10^{-4}. Notice that UHV growth facilities[15,16] have been already used for real-time studies at other synchrotron sources.

The growth of tungsten films was studied in two experiments, which only differed by the value of the grazing incidence angle θ_0 relative to the critical angle for tungsten (0.25° at the energy of 17.5 keV). The angle was set either in the total external reflection (TER) with a θ_0 value of 0.125°, or out of it (OTER) with θ_0 value of 0.5°. The scattering intensity distribution was measured *in situ* as a function of the grazing scattering angle, the sample and the CCD detector both remaining in a stationary position. While tungsten was deposited, a series of scattering diagrams was acquired at 30 s intervals. The integration time of the CCD detector was set to 0.1 s in the case of TER measurements and to 30 s for the less intense OTER measurements. The horizontal beam size was set to 5 mm to favor a high intensity at the detector. As the scattering diagram is very narrow in the azimuthal (horizontal) plane, the scattered intensity was integrated in this direction through pixels binning. The vertical beam size was set to 0.1 mm or 0.2 mm in the case of TER or OTER measurements, respectively.

The two silicon substrates were cut from the same superpolished silicon wafer. From the scattering diagrams of the

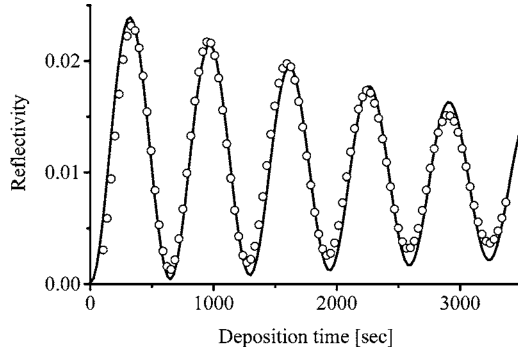

FIG. 2. Reflectivity of a tungsten film versus deposition time. The *in situ* measurements were performed at a grazing angle θ_0 of 0.5° and an energy E=17.5 keV.

substrates measured prior to deposition, we confirmed that both substrates had identical statistical parameters of roughness. Within the measurable spatial frequency range, they could be described by a one-dimensional PSD function having the form of a fractal power law, $PSD_s(p) \sim 1/p^{1+2H}$, with a Hurst exponent H=0.10, leading to an rms roughness value of 0.18 nm. The range of spatial frequencies, $p \in [0.15, 15]$ μm^{-1}, was limited experimentally, on the lower side by the size of the beamstop, and on the higher side, by the size of the transmission silicon detector.

III. DATA ANALYSIS AND DISCUSSION

The evolution as a function of the deposition time of the total integrated reflectivity, i.e., the sum of the specular reflectivity and of the total integrated scattering measured in OTER with the diode transmission detector, is shown in Fig. 2, circles. The solid curve is the result of the fitting assuming a deposition rate of 7.65 pm/s. The decay of the oscillations is caused by the augmentation of absorption while the film grows. The density of the film was found by fitting the reflectivity curve measured after deposition as a function of the grazing angle, and proved to be nearly the same as for bulk tungsten. Although the fitting model did not account for roughness, a good fit of the experimental reflectivity curve is achieved. Because it is redistributing the outgoing intensity between specular reflected and diffuse scattered components, the long-scale roughness does not influence the total integrated reflectivity measured, which differs from the case of specular reflectivity. In turn, the small-scale roughness of the films studied is extremely small and does not exceed a fraction of an angstrom. A series of scattering diagrams measured with the CCD camera in TER and OTER conditions is shown in Fig. 3, circles. The sharp minimum observed on the curves, at the position of the specular peak, is due to the presence of the beamstop.

In the frame of the first-order scalar PT, the scattering diagram integrated over the azimuth scattering angle reads

$$\Pi(\theta,h) = \frac{1}{W_{inc}}\frac{dW_{scatt}}{d\theta} = \frac{k^3}{16\pi \sin\theta_0}[A_f PSD_f(p,h) + A_s PSD_s(p) + A_{sf} PSD_{sf}(p,h)], \quad (1)$$

in which A_f, A_s, and A_{sf} have the following expressions:

$$A_f = |(1-\varepsilon_f)[1+r(\theta_0,h)][1+r(\theta,h)]|^2,$$

$$A_s = |(\varepsilon_f - \varepsilon_s)t(\theta_0,h)t(\theta,h)|^2,$$

$$A_{sf} = 2\,\mathrm{Re}\{(1-\varepsilon_f)(\varepsilon_f-\varepsilon_s)^*[1+r(\theta_0,h)][1 + r(\theta,h)]t^*(\theta_0,h)t^*(\theta,h)\}, \quad (2)$$

where W_{inc} and dW_{scat} are the radiation powers of the incoming beam impinging under an angle θ_0 and of the beam scattered in the θ direction within an angular interval $d\theta$, respectively. The dielectric constants of the substrate and of the film are noted ε_s and ε_f. The amplitude reflectance and transmittance of a perfectly smooth film of thickness h are noted $r(\theta,h)$ and $t(\theta,h)$, respectively. $PSD_f(p,h)$ is the one-dimensional PSD function of the external film surface and $PSD_{sf}(p,h)$ describes the statistical correlation between film roughness and substrate roughness. The quantity $p=|\cos\theta - \cos\theta_0|/\lambda$ is the spatial frequency and $k=2\pi/\lambda$ the wave number.

The PT can only be applied when the samples are very smooth and for a limited range of scattering angles θ. It is usually assumed that PT is valid when the parameter $q_z\sigma = k\sigma(\sin\theta + \sin\theta_0)$ is less than unity,[17] which is the case in our experiments. Nevertheless, when the form of the PSD function follows an inverse power law of the spatial frequency, as for a fractal surface, the PT would be valid over a much wider angular range, as demonstrated in Ref. 13. One should point out that in the analysis of diffuse scattering diagrams, and following the classical paper of Ref. 18, many authors have been using a simplified version of the DWBA formalism that consists of replacing the unperturbed wave field in vacuum by the analytical continuation of the wave field in matter. Within this approximation, the agreement with the exact DWBA may actually be worse than in the case of PT. A more detailed discussion on this issue can be found in Ref. 13.

The expression for the scattered intensity in Eq. (1) is composed of three terms. The first two terms describe the intensity scattered from the film surface and from the substrate, while the third term originates from the interference of the waves scattered by the different interfaces having conformal roughness. By measuring the scattering diagram at two different θ_0 angles, one can use Eq. (1) to form a system of linear algebraic equations. For each value of the spatial frequency p, the two unknown functions $PSD_f(p)$ and $PSD_{sf}(p)$ can then be derived without using any model of correlation function. However, the solving of this system turns out to be an ill-conditioned problem, when even a small inaccuracy in the measured scattering intensity may lead to a very large error in the PSD functions extracted. One way of overcoming the problem is described in Refs. 19 and 20.

However, when the films are thick enough, which is the case in this paper, the extraction of the PSD functions is simpler. In this case, when the probe beam falls onto a sample in the TER condition, the electrodynamics factors A_s and A_{sf} decrease exponentially with increasing film thickness

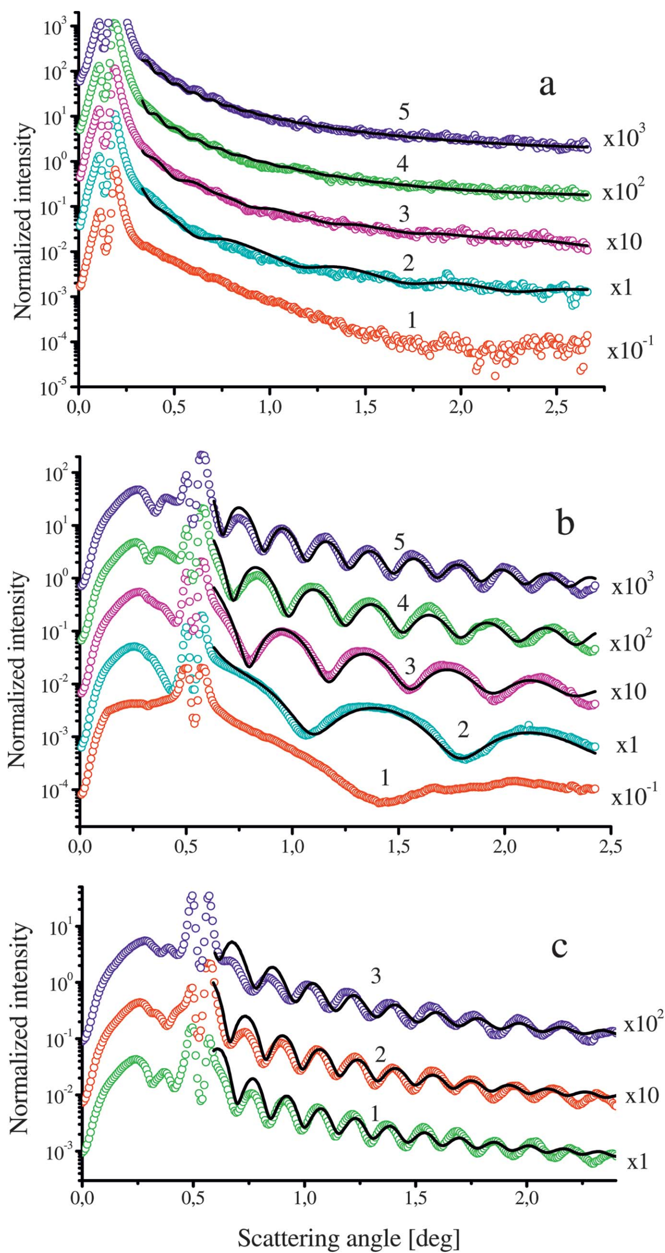

FIG. 3. (Color) Normalized scattered intensity (circles) measured *in situ* in the TER [(a) $\theta_0=0.125°$] and the OTER [(b), $\theta_0=0.5°$] at $E=17.5$ keV and at corresponding film thickness: $h=2.5$ nm (1), 5.6 nm (2), 10.2 nm (3), 14.8 nm (4), 19.4 nm (5), and normalized scattering intensity measured *in situ* in the OTER [(c), $\theta_0=0.5°$] from a film with the thickness $h=23.5$ nm at three x-rays energy $E=19$ keV (1), 17.5 keV (2), and 16 keV (3). The solid curves have been calculated using the PSD functions displayed in Fig. 4. For clarity the curves are shifted vertically.

h. Therefore, when h is of the order of 5–6 nm, the scattered intensity is only caused by the surface roughness of the external film. Thus, neglecting the effect of the substrate ($A_s=A_{sf}=0$), the PSD function of the external film surface $PSD_f(p)$ can be extracted directly from Eq. (1). To get rid of the statistical oscillations, we approximated the PSD functions using the following expression:

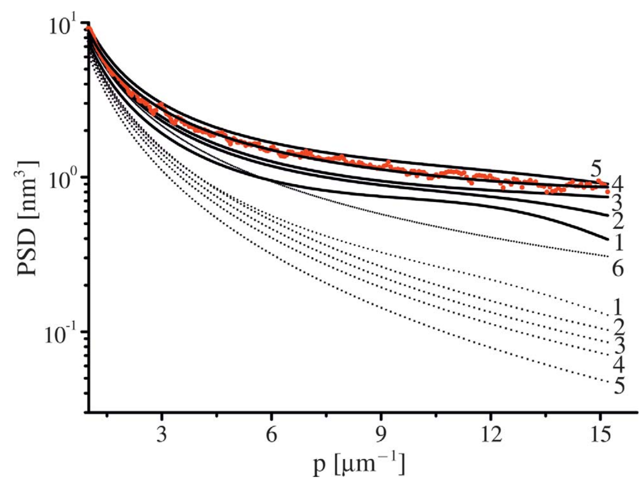

FIG. 4. (Color) PSD functions of the external film surface (solid curves) and of cross-correlation (dotted curves) extracted from the measured scattering diagrams as a function of the film thickness h: 5.6 nm (1), 10.2 nm (2), 14.8 nm (3), 19.4 nm (4), and 23.5 nm (5). Curve 6 is the PSD function of the silicon substrate. Red points represent the PSD function of the 19.4-nm-thick film extracted directly from the scattering diagram measured in the TER condition without polynomial smoothening.

$$\log_{10} PSD_f(p) = \sum_{j=0}^{j_{\max}} a_j(\log_{10}p)^j, \quad j_{\max}=2 \text{ or } 3. \qquad (3)$$

The smoothed PSD functions are shown in Fig. 4, solid curves 1–5, for different film thicknesses. For comparison, the smoothed PSD function of the substrate is also presented (curve 6). Moreover, the PSD function of the 19.4-nm-thick film (red points in the figure) was extracted directly from the scattering diagram measured in TER condition. As one can see, despite the statistical oscillations (no polynomial smoothing), the difference between curves 3, 4, and 5 is definitely distinguishable.

The PSD function of the external film surface increases with film thickness due to the development of intrinsic film roughness. The variation of the PSD function is more pronounced at high spatial frequencies, as also predicted from the existing theories on film growth.[1,2] In the measured range of spatial frequency, this increase in the PSD corresponds to a slight increase of the rms roughness parameter, from 0.18 nm for the bare substrate up to 0.21 nm after deposition of a 23.5-nm-thick film. Although the reason for such a small raise of roughness is not quite clear yet, this property has been already exploited for fabricating tungsten-containing multilayer mirrors. In this case, the excellent x-ray reflectivity values achieved (see, e.g., Ref. 21) demonstrates that thin tungsten layers can be grown keeping an extremely small interfacial roughness. On the other hand, the slow rise of roughness is only observed for thin-enough films, i.e., when the film thickness is smaller than 25 nm. For greater values, a dramatic development of roughness is observed, probably due to tungsten crystallization. For instance, a roughness

value of 2.5 nm was measured by AFM (8 μm scanning window) on a 70-nm-thick film. Notice that the perturbation theory used for extracting the PSDs from the scattering diagrams becomes invalid at this roughness level.

When the probe beam falls onto the sample in the OTER condition, the electrodynamics factor A_{sf} oscillates as a function of the scattering angle θ, the frequency of the oscillations increasing with the film thickness. These oscillations are clearly observed in the measured scattering diagrams presented in Fig. 3(b), thus demonstrating the presence of roughness conformity between the film and the substrate underneath. As the functions $PSD_s(p)$ and $PSD_f(p)$ were already obtained from the TER measurement, it is now possible to extract, from Eq. (1), the PSD function for the cross-correlation $PSD_{sf}(p)$. As above, the PSD functions extracted contained statistical oscillations, which can be large in the vicinity of the spatial frequencies where the factor A_{sf} is equal to zero. To remove them, we used a polynomial approximation of the function $PSD_{sf}(p)$ with coefficients found by the fitting of the scattering diagram in the OTER condition. The resulting smoothened functions $PSD_{sf}(p)$ are presented in Fig. 4, dotted curves 1–5, for different film thickness. The figure demonstrates clearly that conformity of roughness decreases with increasing film thickness and increasing spatial frequency. Finally, using the functions PSD_s, PSD_f, and PSD_{sf} given in Fig. 4, the scattering diagrams corresponding to the TER and OTER regions were calculated (Fig. 3, solid curves) and compared to the measured ones (circles). It is important to emphasize again that these PSD functions were obtained from the measured scattering diagrams without any additional assumption about roughness.

The experimental data were processed beginning from a film 5.6 nm thick. Actually, the scattering from thinner films is not only caused by the external film roughness, but also by the substrate roughness, although measurements are performed in the TER condition. In particular, small oscillations, resulting from the interference between the waves scattered from the film surface and the substrate, can be observed [Fig. 3(a), curve 2]. Below a thickness of 5.6 nm, a model independent analysis of the scattering diagrams would require the development of a more complex procedure of data processing.

To further verify the correctness of our approach, we measured the scattering diagrams from the thickest film (h =23.5 nm) in the OTER condition (θ_0=0.5°) at other x-ray energies E=16 keV and 19 keV [Fig. 3(c)]. The measurements were then compared to the result of calculations performed with the use of the same PSD functions extracted from the measurements at 17.5 keV. The good agreement demonstrates the consistency of the procedure used to extract the PSD functions. A simplified model of film could probably explain the small difference between the calculated and the measured scattering diagrams of Fig. 3. In particular we assumed and a constant density along the tungsten film depth and a constant substrate roughness during deposition. We also considered as negligible the presence of an interlayer between film and substrate. Such interlayer is always arising, resulting from partial implantation and diffusion of tungsten atoms into the silicon substrate.

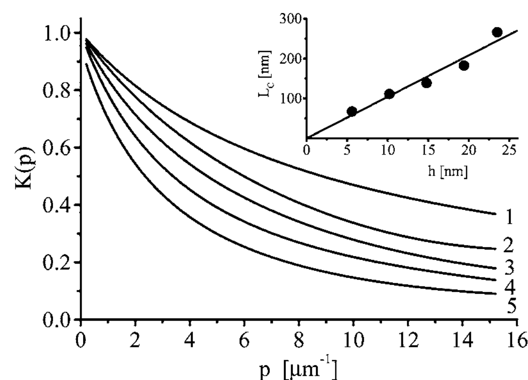

FIG. 5. Replication factor of roughness for different film thicknesses: 5.6 nm (1), 10.2 nm (2), 14.8 nm (3), 19.4 nm (4), and 23.5 nm (5). The inset shows the dependence on the film thickness of the critical length of the roughness replicated.

To characterize the roughness conformity quantitatively, we calculated the replication factor for roughness,

$$K(p,h) = \frac{PSD_{sf}(p,h)}{\sqrt{PSD_f(p,h)PSD_s(p)}}, \tag{4}$$

which is shown in Fig. 5 for different film thicknesses. Let us define the critical spatial frequency $p_c(h)$, for which the replication factor is decreased by a factor e, and the corresponding critical length $L_c(h)=1/p_c(h)$. The dependence of L_c on the film thickness is shown in the inset of Fig. 5. Surface features with a lateral size greater than L_c are strongly replicated after deposition of a film of thickness h. Features with a smaller size are smoothened, although additional uncorrelated roughness appears. As one can see, the critical size of a replicated feature increases proportionally to the film thickness. For the tungsten growth process presented here, only surface features with a lateral size about 10 times greater than the film thickness are well replicated.

IV. CONCLUSION

The experimental method and data treatment presented here can be applied to study a large variety of processes, e.g., thermal evaporation, ion beam-assisted deposition, or ion beam etching. In particular, the *in situ* x-ray characterization system makes the data analysis easier, avoiding in particular surface contamination. For film thicknesses greater than 5–6 nm, it is possible to extract all PSD functions from TER and OTER measurements without assuming any model of surface topography. Future prospects include the study of films of smaller thicknesses (<5 nm) and/or other materials.

ACKNOWLEDGMENTS

The authors gratefully acknowledge the BM5 beamline staff, the SciSoft, and the support groups of the ESRF for technical assistance during the design and realization of the experimental apparatus. Special thanks also to R. Felici, C. Boragno, and F. de Bergevin for useful discussions.

[1] A.-L. Barabâasi and H. E. Stanley, *Fractal Concepts in Surface Growth* (Cambridge University Press, Cambridge, 1995).
[2] D. G. Stearns, Appl. Phys. Lett. **62**, 1745 (1993).
[3] T. Salditt, T. H. Metzger, and J. Peisl, Phys. Rev. Lett. **73**, 2228 (1994).
[4] J. M. Bennett and L. Mattsson, *Introduction to Surface Roughness and Scattering* (Optical Society of America, Washington, DC, 1999).
[5] J. H. Underwood *et al.*, in *OSA Proceeding on Extreme Ultraviolet Lithography* (OSA, WASHINGTON, DC, 1994), p. 61.
[6] V. E. Asadchikov *et al.*, Nucl. Instrum. Methods Phys. Res. A **530** 575 (2004).
[7] T. Salditt *et al.*, Phys. Rev. B **51**, 5617 (1995).
[8] J.-P. Schlomka *et al.*, Phys. Rev. B **51**, 2311 (1995).
[9] J.-P. Schlomka, M. Tolan, and W. Press, Appl. Phys. Lett. **76**, 2005 (2000).
[10] R. K. Heilmann and R. M. Suter, Phys. Rev. B **59**, 3075 (1999).
[11] I. V. Kozhevnikov, Nucl. Instrum. Methods Phys. Res. A **498**, 482 (2003).
[12] E. Spiller, D. Stearns, and M. Krumrey, J. Appl. Phys. **74**, 107 (1993).
[13] I. V. Kozhevnikov, J. X-Ray Sci. Technol. **8**, 253 (2000).
[14] E. Ziegler *et al.*, in *Synchrotron Radiation Instrumentation*, AIP Conf. Proc. No. 705 (AIP, San Francisco, 2004), p. 436.
[15] R. L. Headrick *et al.*, Phys. Rev. B **54**, 14686 (1996).
[16] M. V. R. Murty *et al.*, Phys. Rev. B **60**, 16956 (1999).
[17] W. Press *et al.*, Physica B **221**, 1 (1996).
[18] S. K. Sinha *et al.*, Phys. Rev. B **38**, 2297 (1988).
[19] V. E. Asadchikov *et al.*, Proc. SPIE **3738**, 387 (1999).
[20] V. E. Asadchikov *et al.*, Crystallogr. Rep. **43**, 110 (1998).
[21] http://www.cxro.lbl.gov/cgi-bin/mldata.pl